Evidence from Tropical Raindrop Spectra of the Origin of Rain from Stratiform versus Convective Clouds

ALI TOKAY * AND DAVID A. SHORT

NASA Goddard Space Flight Center, Greenbelt, Maryland

(Manuscript received 12 December 1994, in final form 23 August 1995)

ABSTRACT

An analysis of temporal variations in gamma parameters of raindrop spectra is presented utilizing surface-based observations from the Tropical Ocean Global Atmosphere Couple Ocean-Atmosphere Experiment. An observed dramatic change in the N_0 parameter, found to occur during rainfall events with little change in rainfall rate, is suggestive of a transition from rain of convective origin to rain originating from the stratiform portion of tropical systems. An empirical stratiform–convective classification method based on N_0 and R (rainfall rate) is presented. Properties of the drop size spectra from the stratiform classification are consistent with microphysical processes occurring within an aggregation/melting layer aloft, which produces more large raindrops and fewer small to medium size raindrops than rain from the convective classification, *at the same rainfall rate.* The occurrence of precipitation was found to be 74% (stratiform) and 26% (convective), but total rainfall, on the other hand, was 32% and 68%, respectively. Case studies of the tropical systems studied here indicate that heavy convective showers are generally followed by longer intervals of lighter rain from the stratiform portion of the cloud systems. Differences in the shapes of the frequency distributions of the integral rainfall parameters (i.e., liquid water content, rainfall rate, and radar reflectivity) suggest that the lognormal distribution applies to some, but not all cases. The analysis shows that almost all the precipitation with a radar reflectivity above 40 dBZ falls within the convective classification. Regarding radar reflectivity versus rainfall rate relationships, the exponent is lower and the intercept is higher in the *tropical* stratiform classification than in the *tropical* convective classification. Collision and evaporation rates, which are important for cloud-modeling studies, indicate substantial variation at different rainfall rates and between the two types.

1. Introduction

"Precipitation is generally considered to be of two clearly distinguishable types—stratiform and convective. Stratiform precipitation falls from nimbostratus clouds, while convective precipitation falls from cumulus and cumulonimbus clouds" (Houze 1993). Discussions in the aforementioned reference are followed below in a much abbreviated fashion. The vertical air velocity within clouds plays a crucial role in distinguishing between the two types of precipitation. In stratiform (convective) rain clouds the vertical air velocity is less than (greater than) the terminal velocity of ice crystals and snow ($1-3$ m s^{-1}). The growth of ice crystals in the upper portion of the stratiform clouds is due primarily to vapor deposition where vertical air motion does not exceed a few tens of centimeters per second. The ice crystal growth processes of aggregation and riming can start to occur when the ice particles descend to within about 2.5 km of the freezing level. Aggregation does not add mass to the precipitation but rather concentrates the condensate into large particles, which, upon melting, become relatively *large,* rapidly falling raindrops (Houze 1993). The time required for the growth of precipitation particles in convective clouds is much less than that in stratiform clouds. Therefore, the precipitation particles originate and grow not far from the cloud base. With the existence of strong updrafts, it is possible that the precipitation particles in convective clouds are carried upward and continue to grow until they become heavy enough to overcome the updraft and begin to fall relative to the ground. In convective clouds, growth by accretion of liquid water is the dominant mechanism followed by collisions, coalescence, and breakup of raindrops.

Association of rainfall with stratiform or convective clouds is important in observational, modeling, and remote sensing studies because the microphysical processes described above affect 1) kinematic fields via differing vertical profiles of latent heating and 2) radar rainfall estimation algorithms and cloud-modeling parameterizations via differing raindrop size distributions (DSDs). These topics are important for modeling and remote sensing applications such as the National Aero-

* National Research Council research associate.

Corresponding author address: Dr. Ali Tokay, TRMM Office, NASA Goddard Space Flight Center, Greenbelt, Maryland 20771.
E-mail: tokay@trmm.gsfc.nasa.gov

nautics and Space Administration's (NASA) Tropical Rainfall Measuring Mission (TRMM).

1) Vertical heating profiles resulting from stratiform (convective) precipitation processes peak in the upper (lower) portion of the clouds. The heating (cooling) is largely determined by the condensation (evaporation) associated with the vertical air motions in the convective and stratiform regimes. Melting of snow in the stratiform region and radiative processes also contribute significantly to the net heating. The vertical motion profiles in the stratiform regions show upward motion in the upper troposphere and downward motion in the lower troposphere, while the vertical profiles of convective regions show more variations in both magnitude and shape from study to study (Houze 1982, 1989; Tao et al. 1990, 1993). Profiles of mean divergence of tropical mesoscale convective systems show low-level convergence and midlevel divergence in convective regions and vice versa in stratiform regions (Mapes and Houze 1993).

2) Knowledge of raindrop spectra is required for formulation of rainfall retrieval algorithms utilizing radar remote sensing techniques. For example, the NASA TRMM plans to use a spaceborne radar over the global Tropics beginning in late 1997 to measure rainfall remotely (Simpson et al. 1988). The estimation of rainfall rate R from radar reflectivity Z over the tropical oceans, which cover a substantial part of the equatorial belt (>70%), could be improved by employing different Z–R relations within different precipitation regimes. The parameterization of the drop size distribution, on the other hand, has a direct impact on cloud models. Cloud microphysical processes such as evaporation and collision rate, which both are functions of the DSD, play a crucial role in cloud-modeling studies.

Observations of vertical velocities and hydrometeor fall speeds are rare; therefore, identification of convective and stratiform clouds and accompanying rainfall is usually accomplished by indirect methods. For example, it is well established that the horizontal structure of stratiform clouds is more uniform than that of convective clouds. This feature is widely used to distinguish between the two types by radar (Gamache and Houze 1982; Houze and Rappaport 1984; Churchill and Houze 1984), passive microwave (Kummerow et al. 1991), and infrared and visible (Adler and Negri 1988) satellite studies. In addition, a well-marked radar "bright band" in stratiform clouds can be used as a criterion for discriminating between the types (Williams et al. 1995) as well as validation for the classification (Churchill and Houze 1984).

Simpler threshold methods have been applied to rain gauge data (Austin and Houze 1972; Balsley et al. 1988; Johnson and Hamilton 1988) to distinguish between the two precipitation types. Johnson and Hamilton (1988), in their study of a squall line with a trailing stratiform area, assigned 5-min rainfall rates exceeding 0.5 mm per 5 min to the convective portion of the system, until the rate had decreased to less than or equal to this value, after which the rain was assigned as stratiform (even if later increased). Gamache and Houze (1982), on the other hand, used an echo intensity of 38 dBZ as one of their criteria to distinguish between the two precipitation types such that all the rain above this threshold was assumed to be convective, while a texture algorithm was used to distinguish weaker convective cells from stratiform areas of rain. These simple threshold methods are generally used to compare the results from physically based convective–stratiform algorithms applied to the mesoscale convective systems in which both types of precipitation are observed.

Waldvogel (1974) proposed an empirical model of the relationship between the type of raindrop spectra and the convective activity of the precipitating airmass. By fitting observed DSD to an exponential distribution of the form $N(D) = N_0 \exp(-\Lambda D)$, and observing the time variation of N_0 as well as the radar reflectivity profile, two patterns were found. Low values of N_0 were associated with a bright band overhead, in widespread rainfall without convective activity, while sudden increases of N_0 were correlated with the disappearance of the radar bright band and convective activity. Indications of increasing convective activity were then found to be related to a slow decrease in N_0. Radar reflectivity–rainfall relations of the form $Z = AR^b$ showed A (convective) $< A$ (widespread).

In the present study of tropical raindrop spectra, jumps in N_0 have been found to occur systematically during the transition from heavy rainfall to continuous lighter rainfall and Z–R traces strongly suggest separate relations with A (heavy rain) $< A$ (post-transition light rain). In several such cases, simultaneous infrared satellite observations indicate the presence of a convective mesoscale cluster with a widespread stratiform cloud shield, suggesting that the shift in raindrop spectra is associated with the transition from rainfall originating in convective clouds to rainfall originating from the stratiform portions of the systems. These observations, though from a different meteorological regime than that observed by Waldvogel, suggest a similar behavior and a similar microphysical origin. An empirical classification method based on the variation of N_0 and rainfall rate is developed in the following sections and applied to the data.

The results presented below emphasize the role of large versus small to medium sized raindrops in the size distributions of rain from stratiform versus convective clouds, *at the same rain rate,* particularly in the range of 1–10 mm h^{-1}. It has been found that the size distributions of raindrops in the convective case are characterized by a large number of small to medium sized drops and fewer large drops than the stratiform case at the same rate. This contrast can apparently be attributed to the differing growth mechanisms in the two cloud

types. In the following sections, an analysis of drop size distributions (DSD) observed at Kapingamarangi Atoll (~1.00°N, 154.8°E) during the Tropical Ocean Global Atmosphere Couple Ocean–Atmosphere Experiment (TOGA COARE) intensive observing period (November 1992–February 1993) will be presented. The analysis includes case studies and parameterization of the DSD, distributions of integrated parameters, and calculations of collision and evaporation rates.

2. Data analysis

An RD-69 Distromet disdrometer, located at Kapingamarangi Atoll during the TOGA COARE, provided about 127 h (7605 min) of rainfall with 1-min resolution during the intensive operation period (IOP) of the experiment. Total rainfall recorded by the disdrometer was 535 mm, although some rain events were missed, based on comparisons with a tipping bucket located next to the disdrometer. The tipping bucket gauge, a simple mechanical device, recorded a total rainfall of 525 mm, for the same events recorded by the disdrometer. Although the instrument platform was flooded by a high water event before the IOP began, the raingauge and disdrometer were apparently restored to normal operations as they agree well before and after the event.

The RD-69 disdrometer developed by Joss and Waldvogel (1967) has a sampling cross-sectional area of 50 cm^2 and sorts drops into 20 size intervals ranging from 0.3 to 5.0 mm. The boundaries of 20 channels are adopted following Sheppard (1990), who tested and then corrected the manufacturer's suggested boundaries after his laboratory calibration of the electronics. McFarquhar and List (1993) also found a good agreement with Sheppard's corrected channel widths after performing their laboratory calibration of the electronics. The major problem of the RD-69 disdrometer is its insensitivity to small drops in heavy rain. In the presence of a large number of large raindrops in intense tropical rain ($R \geq 20$ mm h^{-1}), drops smaller than 1.0 mm are underrepresented. This problem is due to an automatic thresholding circuitry that monitors the ambient noise level to reject spurious pulses, but in intense rain the high noise level of the drops themselves is interpreted as ambient noise and small-drop signals are rejected. An algorithm supplied by Waldvogel (Sheppard and Joe 1994) can be used to correct each channel according to the number of impacts in the other channels for the *dead time* of the instrument. The larger drops produce longer dead times and therefore greater corrections. However, the correction algorithm is a multiplication matrix such that it does not increase the counts when the channel has no drops. Unfortunately, this could easily be the case in intense rainfall where the first three to four channels often indicate no drops. Therefore, the dead time correction algorithm was not used in this study. In fact, the underestimation of small raindrops would have an effect on derived relationships of less than 3%. The other sources of errors affecting measurement of small drops, wind and acoustic noise from the surroundings can be reduced to a minimum by a proper installation of the instrument. To avoid the sampling problems, the 1-min samples having fewer than 10 drops or rainfall rates less than 0.1 mm h^{-1} have been excluded from the analysis. The sampling time was also long enough to provide empirical relations between integrated rainfall parameters.

The tipping bucket rain gauge is a reliable instrument to measure the total precipitation. The gauge uses a 20-cm-diameter orifice and a tipping bucket mechanism coupled to a mercury switch. The buckets are calibrated to tip after each 0.254 mm of rainfall. The gauge data is collected with 1-min resolution, therefore, one tip per minute indicates a rainfall rate of 15.24 mm h^{-1}. The gauge may not be too sensitive to very light rain ($R \leq 1$ mm h^{-1}) as well as very heavy rainfall events. Nevertheless, the gauge recorded 76.20 mm h^{-1} (five tips per minute) when rainfall rate reached its maximum 1-min value of 72.35 mm h^{-1} at the disdrometer.

3. Raindrop size distribution

This study of rain originating from convective and stratiform clouds over the warm pool of the western equatorial Pacific Ocean uses microphysical data obtained from a disdrometer which provided 1-min DSD spectra. The widely used gamma distribution function (Ulbrich 1985) was employed for modeling the DSD:

$$N(D) = N_0 D^m \exp(-\Lambda D). \tag{1}$$

A method of moments approach was used to calculate the intercept, N_0 (mm^{-1-m} m^{-3}), slope Λ (mm^{-1}), and shape m parameters (Kozu and Nakamura 1991). For the gamma DSD model, the xth moment of the DSD, M_x, is expressed as

$$M_x = N_0 \frac{\Gamma(m + x + 1)}{\Lambda^{m+x+1}}. \tag{2}$$

Using $x_1 = 3$, $x_2 = 4$, and $x_3 = 6$, the gamma DSD parameters are obtained as follows:

$$m = \frac{11G - 8 + [G(G + 8)]^{1/2}}{2(1 - G)},$$

$$\text{with} \quad G = \frac{M_4^3}{M_3^2 M_6}, \tag{3}$$

$$N_0 = \frac{\Lambda^{m+4} M_3}{\Gamma(m + 4)}, \tag{4}$$

$$\Lambda = \frac{(m + 4)M_3}{M_4} = \frac{(m + 4)}{D_m}, \tag{5}$$

where D_m ($= M_4/M_3$) is the mass-weighted average diameter, and G is the third moment of the mass spectrum normalized by D_m^3.

Calculated rainfall rates from fitted distributions are in excellent agreement with rainfall rates obtained from observed DSDs as shown in Fig. 1. Similar results can also be shown for the other integrated parameters [e.g., liquid water content (M)]. The distribution of the shape parameter was less skewed than that of the intercept and slope parameters as shown in Fig. 2. The mode values of the shape, intercept, and slope parameters were near 6, 3×10^4 mm^{-1-m} m^{-3} and 5.5 mm^{-1}, respectively. It should be pointed out that all three gamma distribution parameters derived from 1-min resolution data are somewhat higher than the ones obtained from time averaged (e.g., half an hour) data. For example, Ulbrich (1985) suggested a range of $-1 \leq m \leq 4$ for the shape parameter.

The method of moments was reapplied for fixed m values and it was found that the root-mean-square error between calculated and observed rainfall rates was minimum (0.05 dB) when the shape parameter was 7 as shown in Fig. 3. This is close to the most probable value shown in Fig. 2. The root-mean-square error for the exponential distribution ($m = 0$), on the other hand, was about 0.20 dB. It should be noted that the underestimation of small raindrops due to the dead time problem of the RD-69 disdrometer causes an overestimation in all three best-fit parameters. For instance, there is a 2%–8% decrease in all three gamma fit parameters when the correction algorithm suggested by Waldvogel is applied.

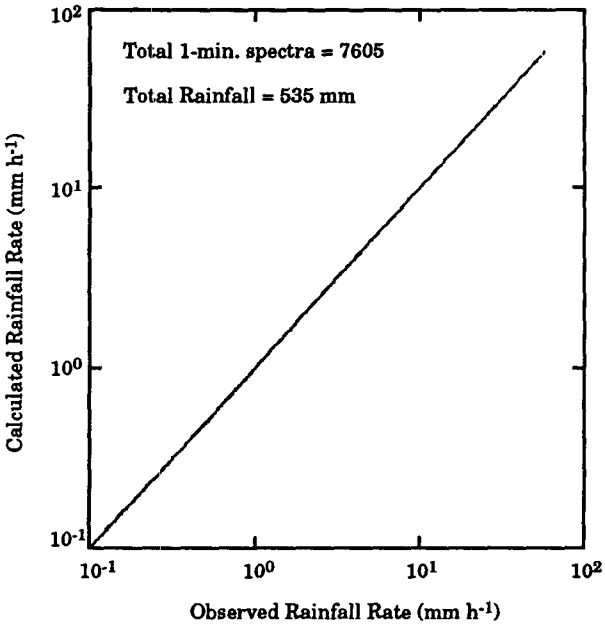

FIG. 1. Observed vs calculated rainfall rate from disdrometer data where "observed" is directly from spectra and "calculated" is from fitted gamma distributions obtained applying the method of moments. Total rainfall and the total number of 1-min spectra are also shown. Note that over 7000 data points, which follow the one-to-one line, are indistinguishable.

As stated earlier, the raindrop size distribution is important in parameterizations of cloud microphysical processes used in the numerical simulation of cloud and larger-scale systems. Traditionally, the precipitation water in microphysical parameterizations is assumed to be distributed exponentially with drop diameter, as suggested by Marshall and Palmer (1948, hereafter MP), $N_0 = 8000$ mm^{-1-m} m^{-3} and $\Lambda = 4.1R^{-0.21}$ mm^{-1}. Although the MP distribution is believed to be a good approximation to the averaged raindrop spectra, it is also understood that MP mainly represents precipitation from stratiform clouds. We categorized the rainfall intensity into six intervals and used an averaged DSD for each category. All three gamma DSD parameters increase with increasing rainfall rate as in Table 1. The MP distribution seems to represent well the gamma fitted DSD in the light and moderate rain categories, while it underpredicts (overpredicts) the upper tail of the distribution in very light (heavy) rainfall. The exponential feature of the MP distribution causes an over prediction of the gamma DSD at the smaller end of the raindrop spectrum in all rainfall rate regimes. It should be pointed out that very similar behavior to the MP distribution was also found in the Sekhon and Srivastava (1971) DSD parameterization even though the latter represents midlatitude thunderstorms (convective precipitation).

4. Development of an empirical classification method

As explained above, rain from nimbostratus clouds in which precipitation particles grow in the ice phase by vapor deposition and aggregation in the upper portion of the cloud reaches the ground with relatively large raindrops, whereas, a large number of small to medium sized raindrops are observed in rain from convective clouds at the same rain rate. As a result, the gamma DSD parameters undergo sudden, independent, very large changes in rainstorms as shown by Waldvogel (1974) and Donnadieu (1982). The former author noticed a dramatic decrease in the intercept parameter (N_0) when a well-defined radar bright band moved over the disdrometer during continuous rain, indicating a level of melting aggregates just below the 0°C isotherm. Rainfall rates were around 5.5 mm h^{-1} in the presence and absence of the bright band. Waldvogel used 1-min as well as averaged DSD over half an hour. Additional evidence of the "N_0 jump" was later provided by Waldvogel et al. (1993). They observed a dramatic decrease in the degree of riming processes in parallel to the decrease in N_0. The degree of riming was determined from the absence of cloud droplets (no riming) and the presence of graupel (fully rimed).

Using 1-min spectra, jumps in N_0 were also observed in this study of tropical DSDs. Figure 4 shows a time series of (a) rainfall rate, (b) a line diagram of R versus N_0, and (c) a line diagram of R versus Z observed on

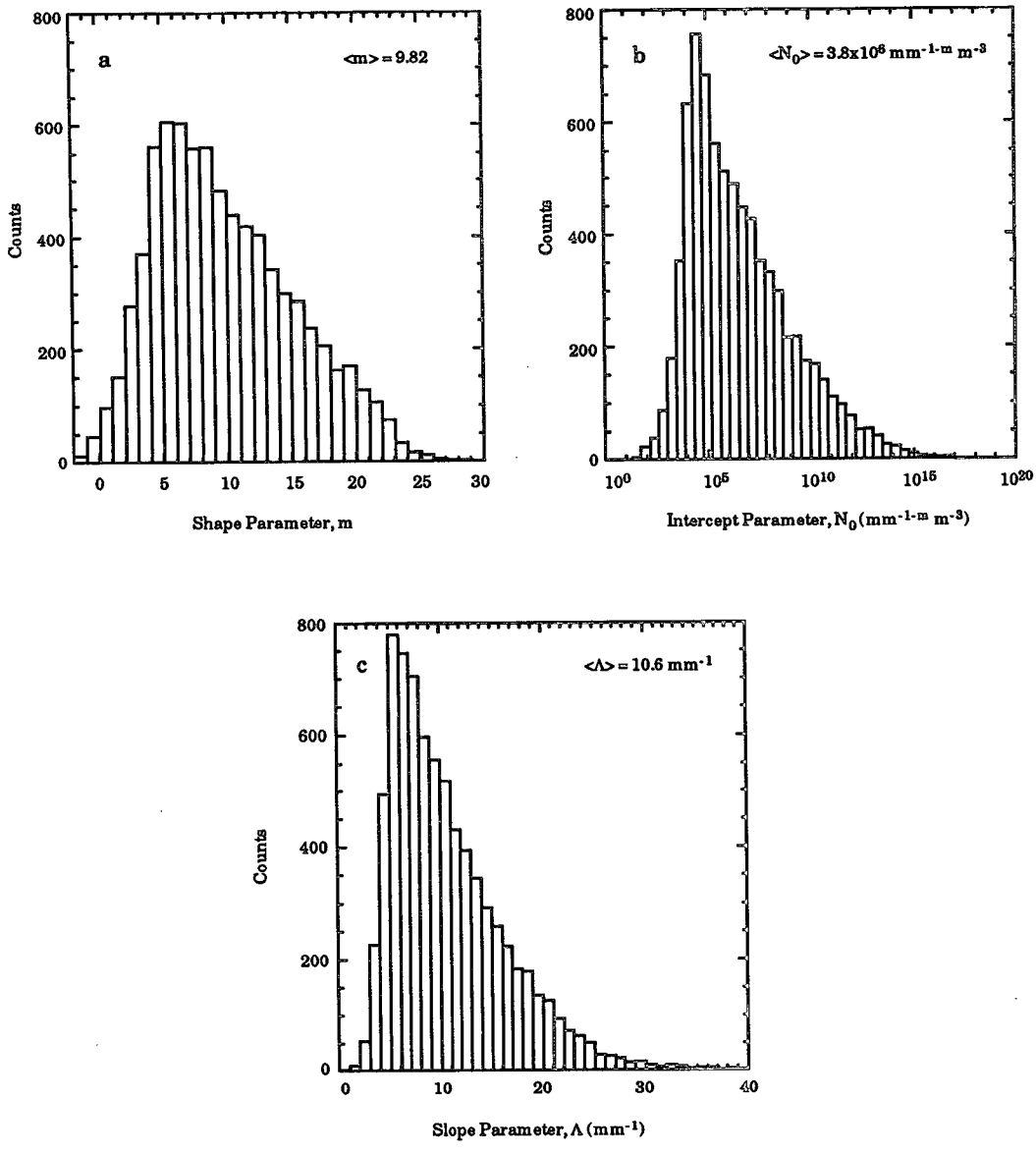

FIG. 2. Distributions of (a) shape, m; (b) intercept, N_0; and (c) slope, Λ, gamma-fitted parameters calculated from the third, fourth, and sixth moments of the observed raindrop spectra as shown in Eqs. (3)–(5). The mean value of each parameter is also shown in the figure. Note that the mean N_0 is calculated as $N_0 = \exp(n^{-1} \Sigma_{i=1}^{n} \log N_{0,i})$.

26 January 1993. Temporally consecutive points are connected in the line diagrams, and it is evident that there are two distinct clusters in both Fig. 4b and Fig. 4c. The upper cluster in Fig. 4b occurs during the initial heavy rains and the lower one during the later light rain. The shift from high to low values of N_0 near a rainfall rate of 5 mm h^{-1} indicates a shift from raindrop spectra dominated by small- to medium-sized drops to spectra dominated by larger drops. This dominance is indicated in Fig. 4c by an increase in Z, the sixth moment of the raindrop size distribution, to the upper cluster of points representing the light rain after 1400 UTC. Because the shift appeared to be more distinct in N_0-R space than in $Z-R$ space in this case and in others, an N_0-R criterion was chosen as a means for classification.

Although the shift in N_0 is not always unambiguous, the line $N_0 = 4 \times 10^9 R^{-4.3}$, was found to separate clusters of points within rainfall events into temporally contiguous groups, identified here as convective (above) and stratiform (below; Fig. 5a). This N_0-R relationship was determined by examination of numerous rainfall events having a substantial increase or decrease in N_0 observed without a large change in rainfall rate. Such temporal shifts in DSD parameters are at-

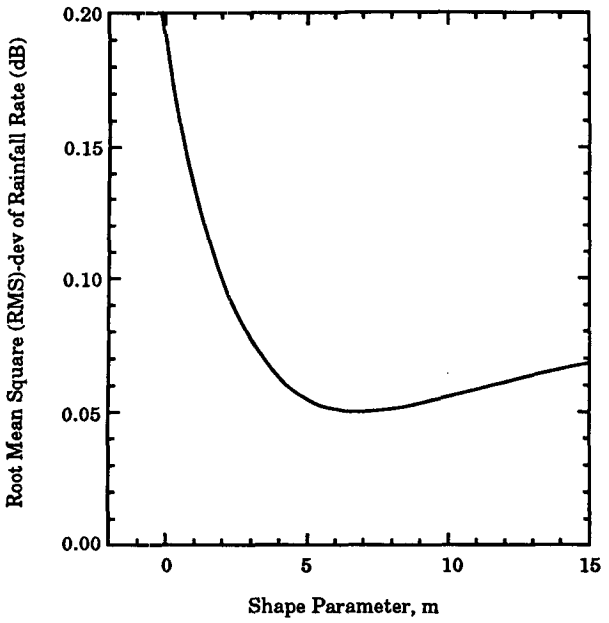

FIG. 3. Root-mean-square error (RMS-dev) of rainfall rate calculated from observed and two-parameter (N_0, Λ) gamma-fitted distributions. The shape parameter is fixed. RMS-dev is calculated as RMS-dev = $10[n^{-1}\sum_{i=1}^{n}(\log R_{\text{est},i} - 10\log R_{\text{meas},i})^2]^{1/2}$.

tributable to shifts in the raindrop size distribution, and by implication, the microphysical processes responsible for their shape. The gamma size distribution, when fit to spectra dominated by a large number of small to medium sized drops with very few larger drops, has large values for N_0, m, and Λ. However, spectra which are dominated by a larger number of large drops give smaller values for all three parameters. This suggests that one can also use $\Lambda = 17R^{-0.37}$ to distinguish between precipitation originating from the two types of clouds (Fig. 5b). Over 98% of the data classified by this $\Lambda-R$ relation agree with the N_0 discrimination technique. It should be noted that a 10% change in either slope or exponent of the N_0-R relation causes only a 1% change in occurrence of the stratiform versus convective classifications by this technique.

It should be mentioned that there are three main differences between the present study and Waldvogel's 1974 study. The drop size distribution here represents solely tropical oceanic precipitation, while Waldvogel collected his data in Locarno on the southern slopes of the Swiss Alps. He used a two parameter (N_0, Λ) exponential DSD, while the three parameter gamma DSD is used in this study. Waldvogel (1974) also examined the qualitative variation of the mean N_0 parameter with respect to convective activity as determined by simultaneous vertical profiles of Z from radar observations, providing independent supporting evidence of his conclusions. His results indicated higher mean N_0 values in weak to medium convection than that in no convection, and a monotonic decrease in the mean N_0 when indications of increasing convective activity were observed. A similar analysis was applied to the tropical N_0 parameter using the two-parameter exponential DSD. It was found that the mean N_0 was lower in the stratiform classification than three different rainfall intervals of convective rain, consistent with Waldvogel's findings. With respect to three convective regimes, the mean N_0 was highest in medium convection ($1 < R \leq 10$ mm h^{-1}) and the lowest for the weak convection ($R \leq 1$ mm h^{-1}).

For all the disdrometer data in the present study, precipitation in the stratiform classification was observed 74% of the time and in the convective classification 26% of time, but total rainfall was 68% convective and 32% stratiform. This is in reasonable agreement with the statistical work done by Bell and Suhasini (1994), who utilized GATE [Global Atmospheric Research Program (GARP) Atlantic Tropical Experiment] phase II gridded rainfall maps derived from shipborne radar data. Their study showed similar percentages found here for the relative area of the radar coverage but had 48% stratiform and 52% convective rain contributions to rain volume. Applying a physically based convective–stratiform algorithm to several GATE squall-line radar fields, it was estimated that 30%–49% of the total precipitation was stratiform (Houze 1977; Gamache and Houze 1983; Houze and Rappaport 1984; Leary 1984). Cloud-modeling studies applied to GATE and EMEX (Equatorial Mesoscale Experiment), suggested 32% (Sui et al. 1994) and 42% (Tao et al. 1993) of total precipitation as originating in stratiform clouds.

A simple threshold technique was applied to the disdrometer-derived radar reflectivity field for comparison with the DSD based convective–stratiform algorithm. Assuming 35 and 38 dBZ as a threshold, below which all the precipitation is assumed to originate from stratiform clouds and vice versa for convective clouds, it was found that both methods are in agreement for 77% and 80% of the data, respectively. Both the 35- and 38-dBZ threshold methods result in less convective rainfall in total occurrence (16% and 8%) and total rainfall (63% and 47%) with respect to the DSD based convective–stratiform algorithm. Similarly, a simple rainfall rate threshold of 6 mm h^{-1} applied to 5-min-averaged disdrometer-derived rainfall rates results in less convective rainfall in total occurrence (14%) and total rainfall (63%). An important distinction between the simplest threshold classifications and more complex ones is that the simplest methods do not allow a rainfall rate interval within which both classifications can be found, whereas the more complex ones indicate that the convective classification exists over a wide range of rainfall intensity from very light to very heavy, as would be expected from convective cells observed over their life cycles, with a wide range of vertical and horizontal extents.

TABLE 1. The gamma raindrop size distribution parameters for different rainfall rate categories.

Category	R (mm h^{-1})	Spectra	N_0 (m^{-3} mm^{-1})	Λ (mm^{-1})	m
very light	$R < 1$	3009 (40%)	5.29×10^3	4.7	1.7
light	$1 \leq R < 2$	1246 (16%)	1.31×10^4	4.7	2.3
moderate	$2 \leq R < 5$	1715 (23%)	2.41×10^4	4.7	2.9
heavy	$5 \leq R < 10$	901 (12%)	8.01×10^4	5.2	3.9
very heavy	$10 \leq R < 20$	392 (5%)	3.32×10^5	6.3	6.1
extreme	$R \geq 20$	342 (4%)	4.26×10^5	6.8	8.9

When the convective–stratiform classification presented here was examined for three rainfall intensity regimes (i.e., light, moderate, and heavy rainfall), the stratiform classification dominated in light rainfall (93% of time when $R \leq 1$ mm h^{-1}), while the convective classification was the main component in heavy rainfall (96% of time when $R > 10$ mm h^{-1}). When the rain rate was larger than 20 mm h^{-1}, all the spectra were found to be convective. This rainfall rate threshold corresponds to 40 dBZ when a GATE Z–R ($Z = 230R^{1.25}$) is applied. Churchill and Houze (1984), who utilized the GATE radar field, used the 40-dBZ threshold as one of their criteria to distinguish the convective and stratiform types such that all the rain above this threshold was assumed to be of convective origin. Convective and stratiform occurrences are more evenly divided when the rainfall rate is between 1 and 10 mm h^{-1}. This is the region where the N_0 jump is most important. Based on the present N_0–R technique a narrow window of rainfall rates around 5 mm h^{-1} was examined. The averaged raindrop spectra of convective and stratiform regimes and best-fitted estimates are shown in Fig. 6. The mean volume diameter D_0 and Z, which represent third and sixth moments of the spectra, increase by 0.37 mm and 3.7 dBZ from convective to stratiform spectra, respectively, while M decreases 0.047 g m^{-3} at the rain rate of 5 mm h^{-1}. This is parallel to the Atlas et al. (1984) statement that "when rain is composed of many small drops of low fall speed, the liquid water content is bound to be higher and the reflectivity lower than with an equal rain rate of larger fast falling raindrops." All three parameters of the gamma DSD have lower values in stratiform spectra than in convective spectra.

A total of 15 major rain events were observed during the interval from 1 November 1992 to 10 February 1993. Given the complexity of structures observed in tropical precipitation systems and the absence of radar observations to determine the propagation, evolution, and spatial structure of the systems responsible for the rain observed at the disdrometer site, some caution should be taken in the interpretation of rainfall-rate time series obtained by point measurements. The representative cases shown in Fig. 7 are presented in order to give the reader some indication of the temporal continuity of the classification.

Case 1, 19 December 1992, showed 11 h of continuous rain (Fig. 7a). The convective classification was dominant, indicating light convective showers until 0700 UTC, followed by heavier showers until 1000 UTC, followed by 4 h of rain with a predominant stratiform classification. Minute-to-minute variations in classification can be seen occasionally in the time series, revealing the empirical nature of the method. Total rainfall recorded by the disdrometer was 64.4 mm and 66.0 mm by the tipping-bucket gauge while the maximum rain rate was 51 mm h^{-1}. Case 2 (Fig. 7b) shows 2 h of predominantly convective rain during a midday event (local time), which preceded the nocturnal event shown in Fig. 4 on the same UTC day. The maximum rainfall rate reached 41.0 mm h^{-1} and total rainfall was 17.2 mm (disdrometer) and 19.8 mm (tipping bucket). A clear separation of the two precipitation types was observed in a light rain event of 5 February 1993 (Fig. 7c). The duration of rainfall was only 3 h and maximum rainfall did not exceed 18 mm h^{-1}. While examination of the time series by itself does not suggest a shift in classification, the N_0 criteria and other measures show that a significant change in the character of raindrop spectra occurred just after 1100 UTC. For example, the calculated reflectivity increased by 4 dBZ, while the rainfall rate remained constant near 3 mm h^{-1}; N_0 decreased by two orders of magnitude, from 10^9 to 10^7 and later to 10^5 (mm^{-1-m} m^{-3}). Total rainfall observed in this case was 13.2 mm by the disdrometer and 13.7 mm by the tipping bucket.

5. Integral rainfall parameters

Integral rainfall parameters, D_0 (mm), M (g m^{-3}), R (mm h^{-1}), and Z (dB) are determined as a function raindrop size distribution as follows:

$$\int_0^{D_0} D^3 N(D)\,dD = \int_{D_0}^{D_{\max}} D^3 N(D)\,dD \qquad (6)$$

$$M = \frac{\rho_w \pi \times 10^{-3}}{6} \int_0^{D_{\max}} D^3 N(D)\,dD \qquad (7)$$

$$R = 6\pi \times 10^{-6} \int_0^{D_{\max}} D^3 V(D) N(D)\,dD \qquad (8)$$

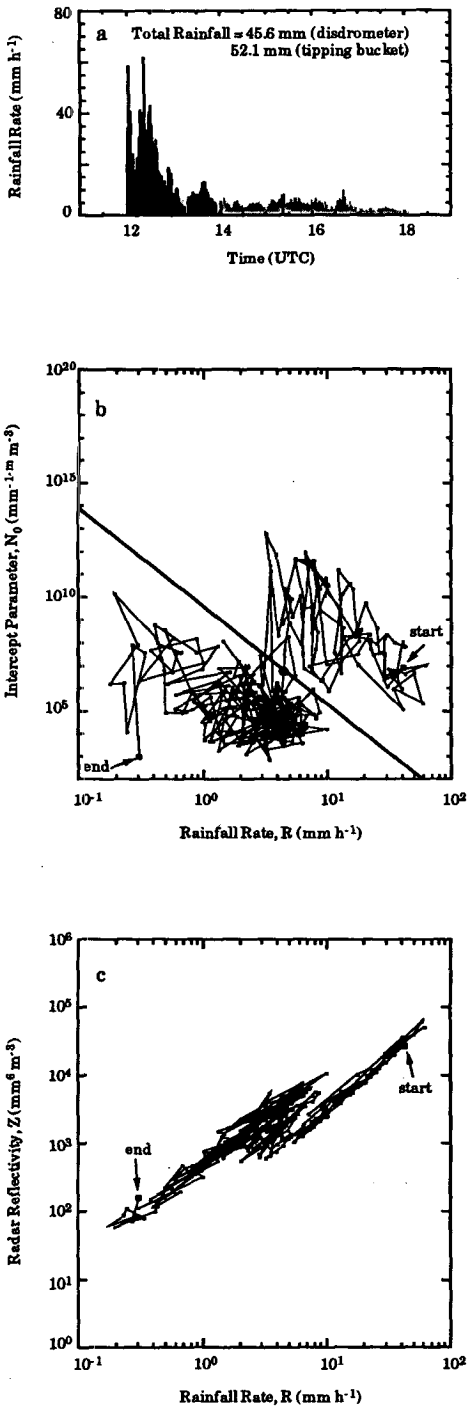

FIG. 4. A case study dated 26 January 1993. (a) Time series of rainfall rate from convective (solid) and stratiform (speckled) clouds. Total rainfall accumulations obtained from the disdrometer and tipping bucket are also shown. (b) Intercept parameter of the gamma drop size distribution as a function of rainfall rate. Note two distinct clusters on each side of the given N_0–R relationship. (c) Radar reflectivity as a function of rainfall rate. Two distinct points of clusters also exist suggesting rain from convective and stratiform clouds. Start and end of the event are shown by arrows in (b) and (c), and the closed circle in (b) represents the transition of rain from convective to stratiform clouds.

$$Z = 10\log(z) = 10\log\left[\int_0^{D_{\max}} D^6 N(D)dD\right], \quad (9)$$

where $V(D)$ (cm s^{-1}) is the terminal velocity of raindrops following Beard (1976), and $D_{\max}$ (mm) is the maximum raindrop diameter.

The median volume diameter, which is a unique function of size distribution parameters, can also be expressed as $D_0 = (3.67 + m)\Lambda^{-1}$. Substituting into Eq. (5), D_0 is also given as a function of mass-weighted average diameter, $D_0 = D_m(3.67 + m)(4 + m)^{-1}$. Ulbrich (1985) showed that D_m is a very good approximation to D_0 for all $m \geq -2$. The mean values of D_0 and D_m calculated from all the data are 1.37 and 1.41 mm, respectively. The frequency distribution of D_0, shown for 0.1-mm intervals in Fig. 8a, reaches about 10% at around 1.15 and 1.35 mm. The width of the distribution is quite narrow, $0.5 \leq D_0 \leq 2.5$ mm for larger than 99% of the data, and $1.0 \leq D_0 \leq 1.8$ mm for 74% of the data. The frequency distributions of M, R, and Z, on the other hand, show a gradual increase toward the peak of the distributions followed by a sharp decrease as in Figs. 8b–d. The mean values of M, R, and Z are -6.7 dBM, 6.2 dBR, and 33.8 dBZ, respectively. The width of the distribution expands toward higher moments of the spectrum, while the peak of the distribution is lower for higher moments. Therefore, the frequency distribution of M has a relatively higher peak and is narrower than the other two, R and Z, and the reverse argument is valid for the frequency distribution of Z. It should be noted that the interval is 2 dBZ in Fig. 8d, while it is 1 dBM, and 1 dBR in Fig. 8b and Fig. 8c. Differences between the shapes of the distributions indicate that the model distributions applied to the observed ones should be different. For instance, the well-known lognormal distribution (e.g., Aitchison and Brown 1957), a normal distribution in log scale, would appear to have a better fit for radar reflectivity than rainfall rate or liquid water content distributions. The limitations of the RD-69 disdrometer in measuring very light rain rate ($R < 0.1$ mm h^{-1}) may play a significant role in fitting lognormal distributions to the M and R distributions, since both are truncated at the lower end of the spectrum.

The frequency distributions of D_0, M, R, and Z for the convective and stratiform classifications are presented in Fig. 9. The convective distribution is shaded in all figures. Both the convective and stratiform distributions of D_0 have a narrow width reaching about 12.5% and 11% at around 1.15 and 1.55 mm, respectively. A quite large area of overlap is shown between distributions of the two types such that the difference between mean values of D_0 for convective and stratiform is only 0.04 mm (0.06 mm for D_m, not shown). The differences in mean values of M, R, and Z are 7.7 dBM, 7.8 dBR, and 7.8 dBZ, respectively. The distributions of M, R, and Z for the stratiform classification are similar to the ones in Fig. 8, while the distributions

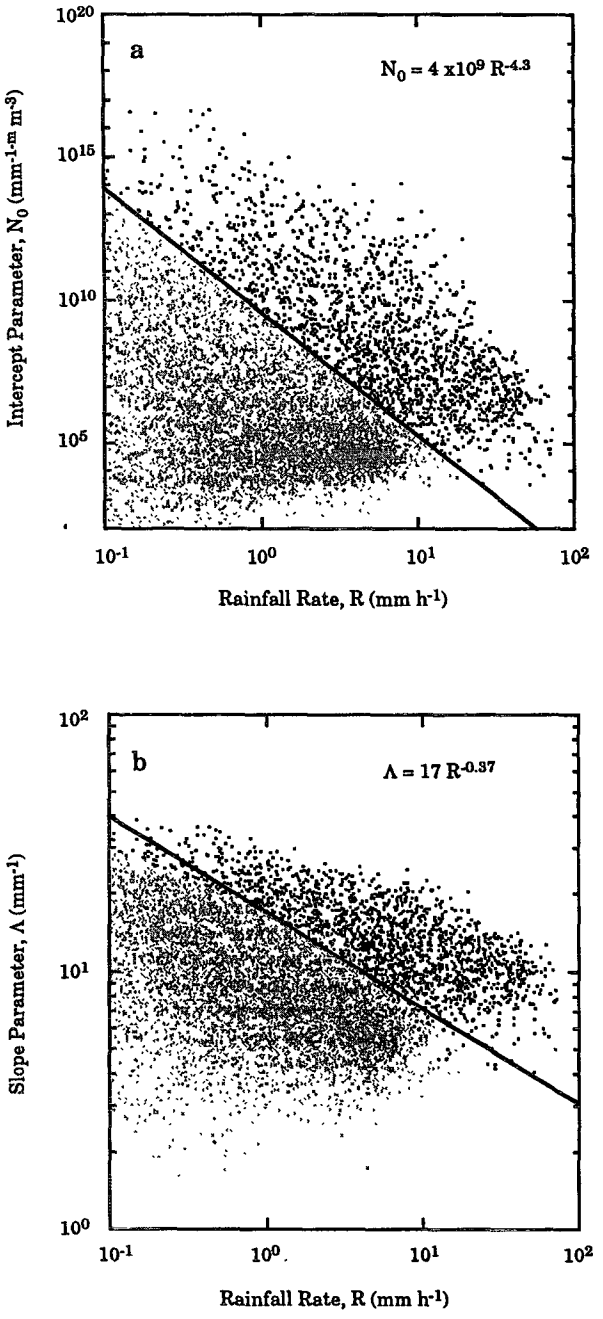

FIG. 5. (a) Intercept and (b) slope parameters of the gamma drop size distribution as a function of rainfall rate. Convective points are heavy and stratiform light. Note that the N_0–R and Λ–R relationships shown as solid lines discriminate between the two types of precipitation.

for the convective classification have higher peaks and narrower widths. The convective distributions exhibit a normal distribution appearance in log space, so that the lognormal fits would be more suitable for the convective distributions than stratiform ones. The upper end of the stratiform distribution of radar reflectivity indicates almost all the data (>99%) above 40 dBZ are convective. As mentioned earlier, this boundary value has been used as a threshold in discriminating cloud types from radar reflectivity analysis by Churchill and

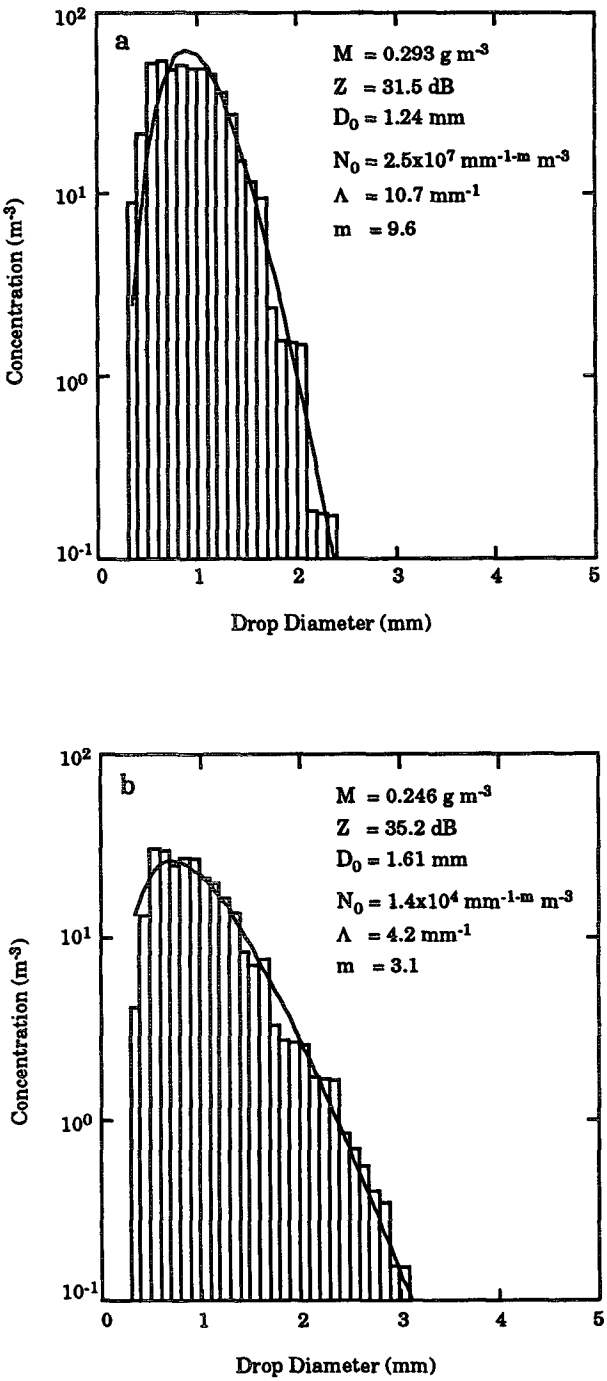

FIG. 6. Observed and fitted composite spectra for (a) convective and (b) stratiform rain from 32 and 40 spectra, respectively, for rainfall rates of approximately 5.0 mm h^{-1}.

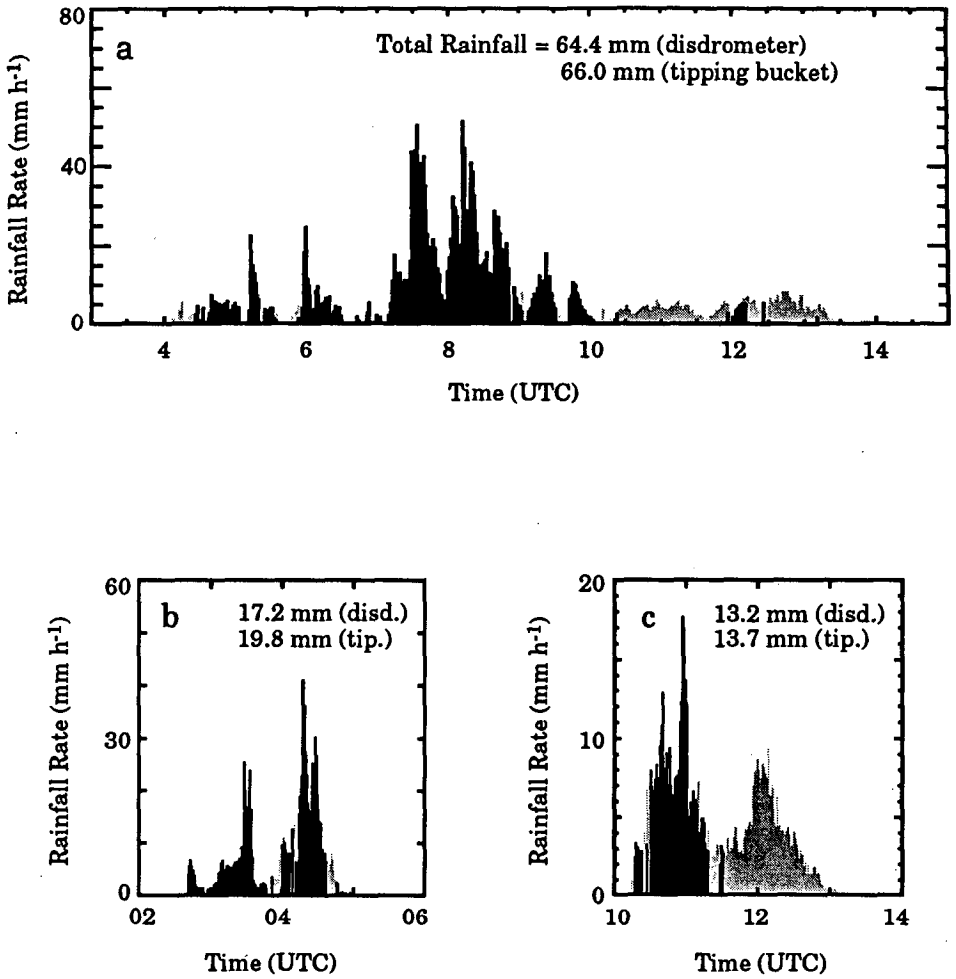

FIG. 7. Time series of rainfall rate on (a) 19 December 1992, (b) 26 January 1993, and (c) 5 February 1993. Solid area indicates convective spectra, and the speckled area is stratiform. Total rainfall accumulations obtained from the disdrometer and tipping bucket shown in the figure agree with each other quite well. Note that case (b) has the same date as in Fig. 4a but it has different time period.

Houze (1984). The problem, of course, is the coexistence of both types below 40 dBZ in radar data. Contoured frequency by altitude diagrams (CFADs), used to show the frequency distributions with height, seem to be a helpful tool to determine cloud and precipitation types from radar data (Yuter and Houze 1995).

The correlation between integral rainfall parameters, M, R, and Z, are above 90% as listed for all convective and stratiform classifications in Table 2. All the relations were obtained in log–log space applying the least squares method. The 95% confidence intervals for the exponents of the stratiform and convective classifications are 0.01; therefore, their difference (1.43 − 1.30 = 0.13) is statistically significant. The relations are highly weighted by the dense observational regime of the independent variable. For instance, rainfall rates are less than 5 mm h^{-1} 79% of the time. This has a lowering effect on the exponent such that in all relations in Table 2, a lower exponent is observed for all the data than the one for both convective and stratiform classifications except for the $M-R$ relations. Therefore, a single $Z-R$ from all the data may not be a good representative for heavy rainfall, rather a separate $Z-R$ must be used for the convective classification. The relations for the stratiform classification are valid up to about 12 mm h^{-1} (40 dBZ), since almost no cases are observed above these limits with a few exceptions as shown in Figs. 9c,d. The relationships for $Z-M$ and $Z-R$, shown in Fig. 10, indicate a lower intercept and higher exponent for the convective classification. These features will be discussed in the following section. It should be noted that the least squares relations are also not self-consistent—that is, they differ from the $Z-R$ mathematically derived from the DSD parameterization. In addition, they differ from the relations that retrieve the first and second moments of the independent

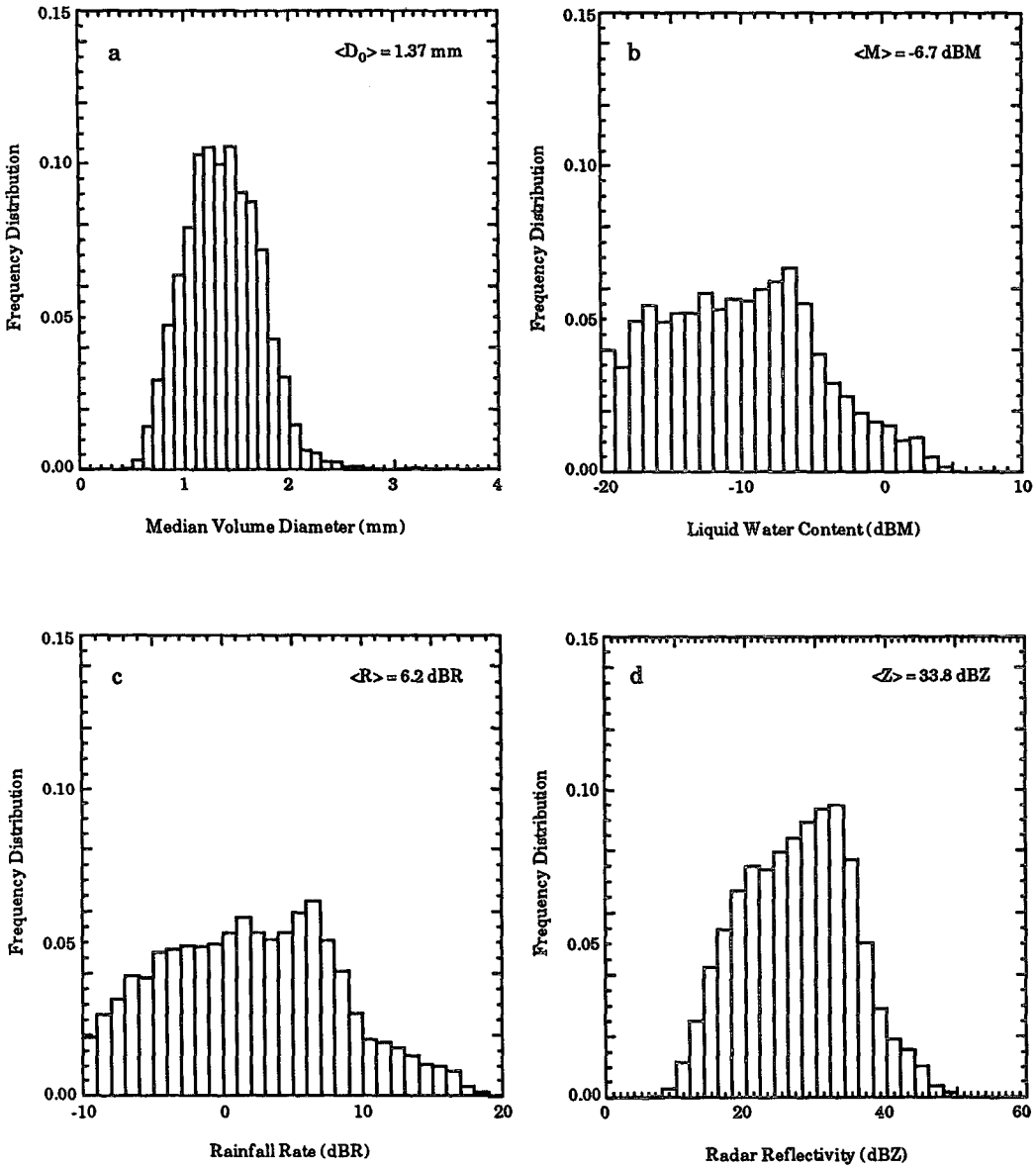

FIG. 8. Distributions of four integral rainfall parameters: (a) median volume diameter D_0, (b) liquid water content M, (c) rainfall rate R; and (d) radar reflectivity Z for all the data. The mean value of each integral parameter is also shown in the figure. Note that the interval is 0.1 mm for D_0, 1 dBM, and 1 dBR for M and R, and 2 dBZ for Z.

variable. These issues have been discussed by Tokay et al. (1995).

Empirical relations between rainfall rate and radar reflectivity have been studied for the last five decades. Battan (1973) reported 69 $Z = AR^b$ relations from many places around the world. Fujiwara (1965), on the other hand, introduced the range for the intercept A and exponent b for thunderstorms, rain showers, and continuous rain. The results from Fujiwara as well as from Jones (1956) and Joss and Waldvogel (1969) show a high intercept ($A > 450$) for thunderstorms (convective) and relatively low intercept for continuous rain (stratiform classification) as in Fig. 11. Our convective and stratiform $Z-R$ relations contradict their findings; that is, high intercept for stratiform and lower intercept for convective rain. The $Z = 200R^{1.60}$ of Marshall and Palmer (1948), which represents midlatitude stratiform conditions, has a very high exponent and relatively low intercept compared to our stratiform $Z-R$. The $Z = 300R^{1.35}$ of Sekhon and Srivastava (1971), observed in midlatitudinal thunderstorms, as well as $Z = 300R^{1.40}$ of NEXRAD (Next Generation Weather Radar) have lower exponents and higher intercepts than our convective $Z-R$. The shipborne dis-

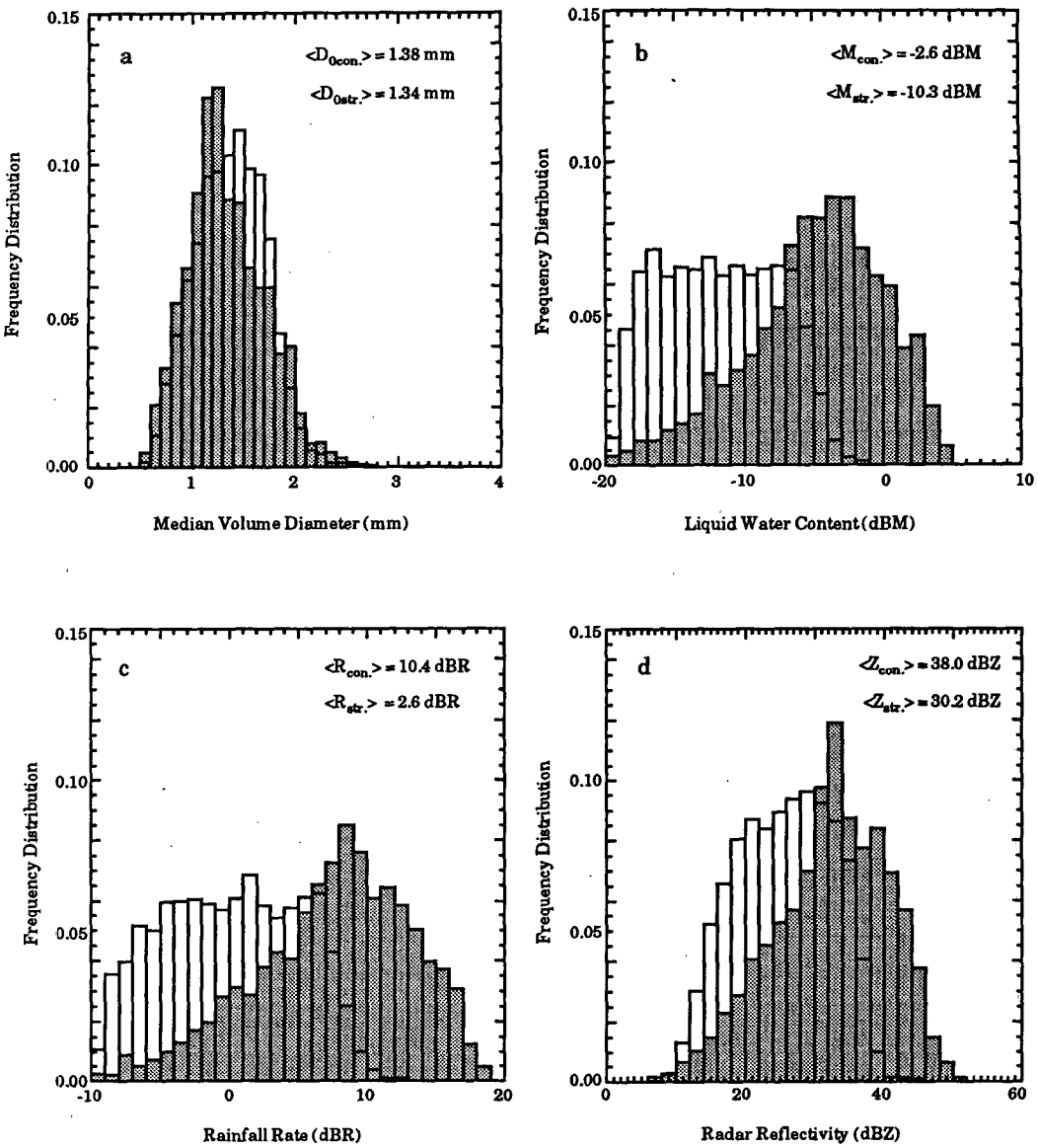

FIG. 9. Same parameters as Fig. 7 but for convective (shaded) and stratiform (clear) precipitation. The mean values for the stratiform and convective rain are also shown.

drometer based GATE $Z-R$ (Hudlow 1979) has a lower intercept and slightly higher exponent than the single TOGA COARE $Z-R$. The $Z = 276.7R^{1.29}$ of Willis (1984), which was reported based on aircraft based disdrometer data taken during flights over Hurricane Anita and Hurricane Frederic off the Florida coast, differs substantially from our convective $Z-R$. This is perhaps not surprising, given the significant occurence of rainfall produced by stratiform clouds in hurricanes. Our convective case closely agrees with the study done by Short et al. (1990), which suggested $Z = 170R^{1.47}$ for convective cases in Darwin, Australia. This provides additional evidence on low intercepts and high exponents in $Z-R$ relationships for precipitation originating from *tropical* convective clouds and vice versa for stratiform, whereas Sauvageot (1994) stated the reverse order for both intercept and exponent when he compared precipitation from *midlatitude* stratiform clouds to a *tropical* squall line.

As an alternative method to least squares fitting using all data points in obtaining the relationships between integral rainfall parameters, a probability matching method was applied to six different percentage values of each parameter given in Table 3. From the matched percentiles of each parameter, a linear least squares fit was then used to calculate power-law relations. The

TABLE 2. Relations between integrated rainfall parameters.

Parameter	Case 1 (all)	Case 2 (convective)	Case 3 (stratiform)
M–R	$M = 0.059R^{0.93}$	$M = 0.074R^{0.86}$	$M = 0.056R^{0.91}$
Z–M	$Z = 1.06 \times 10^4 M^{1.23}$	$Z = 1.01 \times 10^4 M^{1.62}$	$Z = 1.74 \times 10^4 M^{1.34}$
Z–R	$Z = 315R^{1.20}$	$Z = 139R^{1.43}$	$Z = 367R^{1.30}$
D_0–M	$D_0 = 1.61M^{0.08}$	$D_0 = 1.61M^{0.20}$	$D_0 = 1.82M^{0.11}$
D_0–R	$D_0 = 1.26R^{0.10}$	$D_0 = 0.93R^{0.19}$	$D_0 = 1.33R^{0.13}$
D_0–Z	$D_0 = 0.66Z^{0.11}$	$D_0 = 0.45Z^{0.14}$	$D_0 = 0.63Z^{0.13}$

probability matching method is powerful especially when two parameters are independently observed, for instance, the comparison between rain gauge rainfall rates and radar reflectivities (Atlas et al. 1990). A high correlation is again obtained between integral rainfall parameters, choosing five (10%, 25%, 50%, 75%, and 90%) values of the cumulative distributions. Both intercept and exponents obtained for the two different methods are quite close. For instance, the probability matching method suggests $Z = 292R^{1.20}$, $Z = 134R^{1.34}$, and $Z = 367R^{1.30}$ for case one (all), case two (convective), and case three (stratiform), respectively. The minimum and maximum bounds of each parameter are also presented in Table 3.

6. Collision and evaporation rate

Microphysical processes in clouds have a fundamental importance in cloud-modeling studies. For example, the profiles of vertical heating, which have a great impact in forcing the controlling large-scale circulation, are largely determined by microphysical processes in the clouds. The model-generated vertical profile of hydrometeors varies substantially during the lifetime of tropical mesoscale convective systems, depending upon the existence of the convective or stratiform stage cloud (Tao et al. 1990). The size distribution of the hydrometeors, which undergoes a considerable variation during the lifetime of the mesoscale convective system, plays a key role in parameterization of the microphysical process. For example, the two main raindrop growth processes, condensation growth/evaporation and collision/coalescence, are functions of raindrop spectra. The results from the collision and evaporation rates calculated from DSDs of stratiform and convective regimes are presented in this section.

When two raindrops collide, they can either coalesce, bounce off one another, or break into fragments. The rate of collision depends on the size and corresponding terminal velocities of the collector, $V(D)$, and small raindrop, $V(d)$. The number of collisions of a particular D-size drop with all smaller d-size drop is expressed as follows (Johnson and Beard 1984):

$$C(D, d) = n(D) \sum_d \left(\frac{\pi}{4}\right) \times (D + d)^2 [V(D) - V(d)] n(d), \quad (10)$$

where $n(D)$ and $n(d)$ are the number concentrations of large and small raindrops. The collision rate of convective rain is higher than that of stratiform rain. The number of collisions reaches 10 s^{-1} m^{-3} at high rainfall rates. On the average, the collision rates are 0.9 and 0.08 s^{-1} m^{-3} for convective and stratiform precipitation, respectively. The order of magnitude of collision rate ranges between 10^{-4} and 10^0 for stratiform rain and between 10^{-3} and 10^1 s^{-1} m^{-3} for convective rain (Fig. 12a).

The rate of evaporation of a drop falling at terminal velocity in air (dm/dt) is calculated as a function of raindrop spectra following Pruppacher and Rasmussen (1979)

$$\frac{dm}{dt} = f_v 2\pi d D_{v,a} (\rho_{v,e} - \rho_{v,a}), \quad (11)$$

where f_v is the ventilation coefficient, $D_{v,a}$ is the diffusivity of water vapor in air at the drop surface temperature, d is the raindrop diameter, and $\rho_{v,e} - \rho_{v,a}$ is the difference of the density of air at the environment and drop surface. The ventilation coefficient is a function of both Reynolds and Schmidt numbers. The former number is the ratio of inertial force to dynamic viscosity, while the latter number is the ratio of kinematic viscosity to diffusivity.

The evaporation rate presented here is calculated for a 1°C difference between the drop surface and its environment assuming an environmental temperature of 30°C (Fig. 12b). The maximum evaporation rate is 3.6 $\times$ 10^{-3} g s^{-1} m^{-3} and the average rates for the convective and stratiform classifications are 8.8 $\times$ 10^{-4} and 1.7 $\times$ 10^{-4} g s^{-1} m^{-3}, respectively. The relatively high evaporation rates in the convective compared to the stratiform classification was also observed via a sensitivity simulation of a GATE mesoscale system by Ferrier et al. (1995). In model simulations, the parameterization of the DSD plays an important role in allowing the rain from stratiform clouds to reach the surface without undergoing substantial evaporation. A two order of magnitude increase is observed in evaporation rate with increasing rainfall rates for both convective and stratiform classifications. It should be noted that

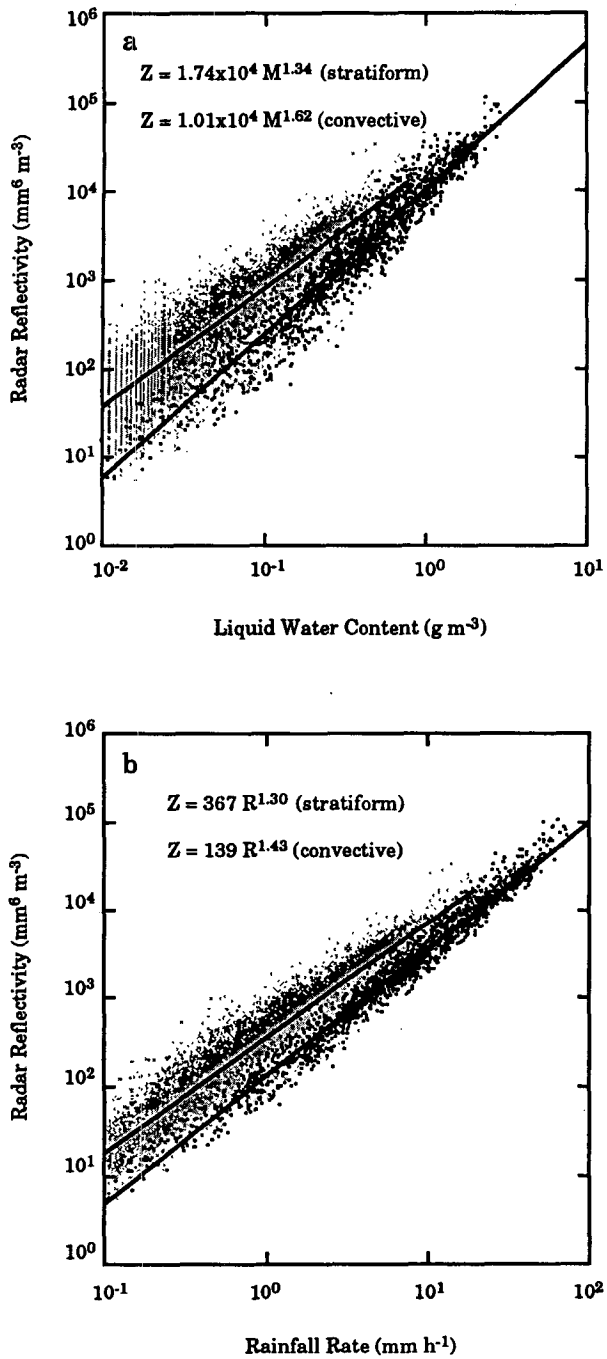

FIG. 10. (a) Radar reflectivity vs liquid water content, and (b) radar reflectivity vs rainfall rate, both calculated from observed spectra. Convective points are heavy and stratiform light, with corresponding Z–M and Z–R relationships shown as solid lines. Note that the stratiform line (b) is above the convective line, indicating higher reflectivities in stratiform rain *at the same rain rate.*

the evaporation rate is very sensitive to the temperature difference between the drop surface and its environment, for instance, the use of a 10°C difference results in an order of magnitude increase in evaporation rates. However, in a very humid environment such as in the tropical Pacific warm pool, the temperature difference between the drop surface and its environment would be expected to be less than 10°C.

7. Conclusions

The classification of two types of precipitation regimes, convective and stratiform, based on microphysical data are determined. Drop size distribution data collected with an RD-69 disdrometer during a tropical field experiment, namely TOGA COARE, is used to determine the classification. Three-parameter gamma-fitted distributions are applied to each 1-min observed raindrop spectra. A very good agreement is obtained between the observed and calculated rainfall rate when the method of moments is used for gamma-fitted distributions. The frequency distributions of both slope and intercept parameters have a sharp increase to their single peak value followed by a gradual decrease, while the shape parameter exhibits a relatively more uniform appearance. The minimum root-mean-square error occurs at around $m = 7$ when m is fixed. This is about 3 less than the mean m of the three-parameter gamma distribution.

A relationship between intercept parameter and rainfall rate (N_0–R) is determined from dramatic decreases

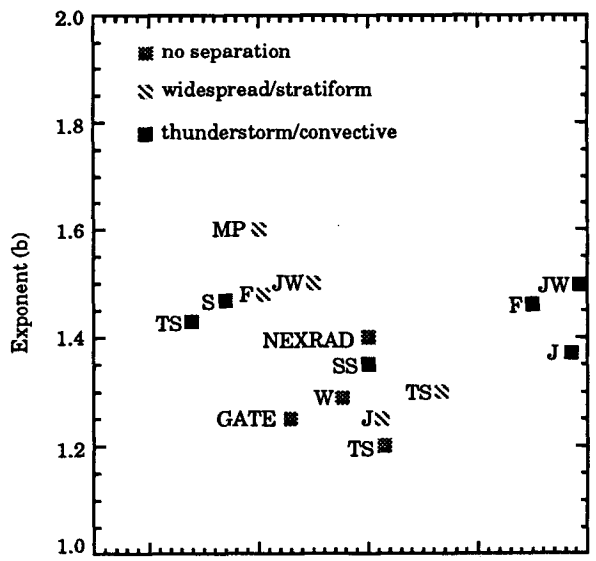

FIG. 11. Summary of the $Z = AR^b$ relations. The following abbreviations are used: JW: Joss and Waldvogel (1969), J: Jones (1956), F: Fujiwara (1965), S: Short et al. (1994), MP: Marshall and Palmer (1948), SS: Sekhon and Srivastava (1971), W: Willis (1984), GATE: Global Atmospheric Research Program (GARP) Atlantic Tropical Experiment (Hudlow 1979), NEXRAD: Next Generation Weather Radar, and TS: Tokay and Short.

TABLE 3. Accumulative percentage, minimum and maximum of the integrated rainfall parameters.

Percent greater than	D_0 (mm)			M (g m^{-3})			R (mm h^{-1})			Z (dB)		
	All	Con.	Str.	All	Con.	Str.	All	Con.	Str.	All	Con.	Str.
10	0.92	0.88	0.93	0.015	0.067	0.013	0.23	0.90	0.20	16.7	20.7	16.1
25	1.11	1.08	1.13	0.030	0.170	0.024	0.50	2.50	0.38	21.3	27.1	20.1
50	1.36	1.28	1.38	0.088	0.378	0.057	1.55	6.60	1.02	27.7	32.9	25.9
75	1.61	1.58	1.62	0.229	0.741	0.138	4.39	14.47	2.64	31.1	38.3	31.1
90	1.81	1.85	1.80	0.518	1.325	0.231	9.69	28.58	4.65	37.0	42.6	34.7
Min	0.47	0.54	0.47	0.006	0.010	0.006	0.10	0.10	0.10	7.3	7.3	7.5
Max	3.22	2.73	3.22	2.945	2.945	0.739	72.35	72.35	17.96	50.4	50.4	45.4

or increases in N_0 during rainfall events with little change in rain rates. Similar changes are also observed in the slope (Λ) parameter, so one can also use a $\Lambda-R$ relation to determine the classification. The relations given here were derived from about 100 days of rainfall data at Kapingamarangi atoll located in the western equatorial Pacific. They do not necessarily represent the climatology of the region. Long-term observations of rainfall and DSD parameters, in addition to vertical reflectivity profiles—that is, at least several years—may be needed to produce the climatology of classifications for a particular region, and to validate the DSD-based classification presented here. Preliminary analysis of Kapingamarangi DSD data suggests that an increase in upper-level moisture results in stratiform spectra with a greater supply of larger drops, increasing the magnitude of the N_0 difference. This could perhaps be due to enhanced growth of aggregates, leading to a larger supply of bigger raindrops after melting. While the N_0-R or $\Lambda-R$ relations are subject to change from one region to another, the "N_0 jump," which results from a shift in the DSD from small to large raindrops, has been previously reported (Waldvogel 1974; Waldvogel et al. 1993). They have shown the N_0 jump in the presence or absence of a radar bright band and from the degree of riming, respectively. Evidence for similar shifts in tropical DSDs can be seen in Zawadski and Antonio (1988) and Hoepffner et al. (1989).

The averaged drop size distributions of the stratiform and convective classification at rainfall rates of 5 mm h^{-1}, have relatively more larger drops and fewer small to medium size raindrops for the former spectrum and vice versa for the latter. There is an increase in liquid water content and decreases in medium volume diameter and radar reflectivity from stratiform to convective spectra. Time series of rainfall rates generally show that rain in the convective classification falls first followed by rain in the stratiform classification within mesoscale systems containing both types of precipitation.

The shape of the frequency distributions of integral rainfall parameters differ from each other and the log-normal model distribution would appear to have a better fit for radar reflectivity than rainfall rate and liquid water content and also a better fit for the convective classification than for the stratiform one. The truncation of the disdrometer data at a lower bound (i.e., the distributions having $R < 0.1$ mm h^{-1} are not included in the analysis) is clearly seen in the rainfall rate and liquid water content distributions. The distribution of radar reflectivity for the stratiform classification suggests that radar reflectivities larger than 40 dBZ most likely represent precipitation of convective origin. The relationship between radar reflectivity and rainfall rate has a lower exponent when all of the data is considered than when it is derived for convective and stratiform cases. This is because the frequency distribution of the independent variables are highly weighted toward the lower end of the spectrum. The disdrometer-derived radar reflectivity versus rainfall rate relationship for the convective classification has a lower intercept and higher exponent than for the stratiform classification in the western tropical Pacific Ocean. This agrees with the results found for Darwin, Australia (Short et al. 1990), but it differs from the comparison of a midlatitude stratiform system versus a tropical squall line (Sauvageot 1994).

The use of dual $Z-R$ and dual $Z-M$ relations will improve the estimation of liquid water content and rainfall rate from radar reflectivity fields. The use of a single $Z-R$ or $Z-M$ underestimates rainfall rate and liquid water in heavy convective showers. The use of a convective $Z-R$ or $Z-M$, on the other hand, overestimates both quantities in stratiform regions. This feature is also seen in numerical cloud model simulations (as identified in Ferrier et al. 1995). The cloud microphysical processes are very sensitive to DSDs. A wide change of collision and evaporation rate is observed at any given rainfall rate. The DSDs corresponding to the convective classification have, on average, higher collision and evaporation rates that the stratiform DSDs. The DSD parameters have a great impact on the rain from stratiform clouds reaching the surface without undergoing substantial evaporation in cloud model simulations.

The convective–stratiform algorithm presented here is based on DSD parameters and is consistent with the current understanding of the microphysics of convec-

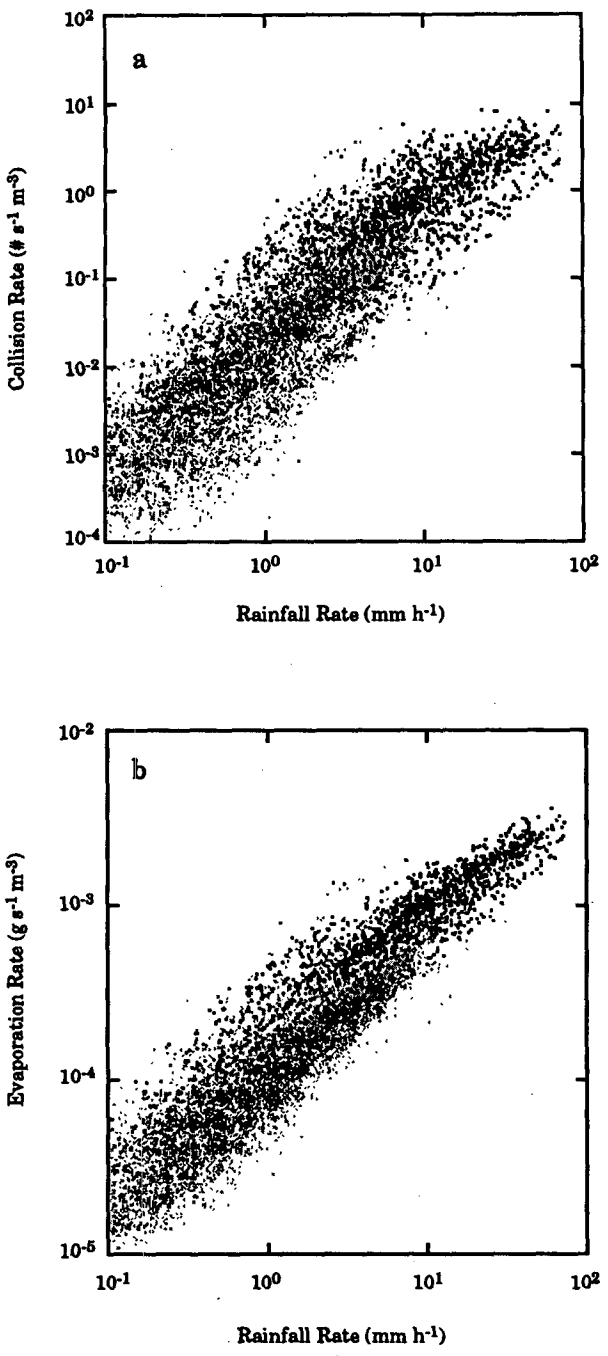

FIG. 12. (a) Collision rate and (b) evaporation rate as a function of rainfall rate. Convective points are heavy and stratiform light. Note that the evaporation rate has relatively more distinct regimes for convective and stratiform precipitation than the collision rate.

tive versus stratiform clouds (i.e., more small to medium size and fewer large raindrops in convective clouds and vice versa in stratiform, *at the same rain rate*). In addition, the method results in classification sequences of convective first, followed by trailing stratiform in mesoscale convective systems. Future studies will focus on intercomparisons of the DSD-based convective–stratiform algorithm with other independent algorithms. In fact, a 915-MHz wind profiler–based convective–stratiform algorithm developed by Williams et al. (1995) is currently being compared with the method presented here. The wind profiler provides vertical profiles of the equivalent reflectivity, Doppler velocity, and spectral width. Additional studies utilizing coincident disdrometer and surface radar data from TRMM validation sites will be reported on at a later date.

Acknowledgments. Thanks to Mr. Otto Thiele of the TRMM Office at NASA Goddard Space Flight Center for his vision and efforts in providing for the disdrometer and other rainfall observations during TOGA COARE. Discussions with Drs. David Atlas and Brad Ferrier of NASA Goddard Space Flight Center; Dr. Brian Sheppard of Atmospheric Environment Service in Downsview, Ontario, Canada; and Dr. Toshiaki Kozu of the Communications Research Laboratory in Tokyo, Japan, were very helpful at different stages of this research. Acknowledgments extend to Prof. Roland List of the University of Toronto and two anonymous reviewers for their constructive criticisms. One of us (Ali Tokay) acknowledges the National Research Council for providing a research associateship.

REFERENCES

Adler, R. F., and A. J. Negri, 1988: A satellite infrared technique to estimate tropical convective stratiform rainfall. *J. Appl. Meteor.*, **27,** 30–51.

Aitchison, J., and J. A. C. Brown, 1957: *The Lognormal Distribution.* Cambridge University Press, 176 pp.

Atlas, D., C. W. Ulbrich, and R. Meneghini, 1984: The multiparameter remote measurement of rainfall. *Radio Sci.*, **19,** 3–22.

——, D. Rosenfeld, and D. B. Wolff, 1990: Climatologically tuned reflectivity–rain rate relations and links to area-time integrals. *J. Appl. Meteor.*, **29,** 1120–1135.

Austin, P. M., and R. A. Houze, 1972: Analysis of the structure of precipitation patterns in New England. *J. Appl. Meteor.*, **11,** 926–935.

Balsley, B. B., W. L. Ecklund, D. A. Carter, A. C. Riddle, and K. S. Gage, 1988: Average vertical motions in the tropical atmosphere observed by a radar wind profiler on Pohnpei (7°N lat, 157°E long). *J. Atmos. Sci.*, **45,** 396–405.

Battan, L. J., 1973: *Radar Observations of the Atmosphere.* University of Chicago Press, 324 pp.

Beard, K. V., 1976: Terminal velocity and shape of cloud and precipitation drops aloft. *J. Atmos. Sci.*, **33,** 851–864.

Bell, T. L., and R. Suhasini, 1994: Principal modes of variation of rain-rate probability distributions. *J. Appl. Meteor.*, **33,** 1067–1078.

Churchill, D. D., and R. A. Houze, 1984: Development and structure of winter monsoon cloud clusters on 10 December 1978. *J. Atmos. Sci.*, **41,** 933–960.

Donnadieu, G., 1982: Observation de deux changements des spectres des gouttes de pluie dans une averse de nuages stratiformes. *J. Rech. Atmos.*, **16,** 35–45.

Ferrier, B. S., W. K. Tao, and J. Simpson, 1995: A double-moment multiple-phase four-class ice scheme. Part II: Simulations of convective storms in different large-scale environments and

comparisons with other bulk parameterizations. *J. Atmos. Sci.*, **52,** 1001–1033.

Fujiwara, M., 1965: Raindrop-size distribution from individual storms. *J. Atmos. Sci.*, **22,** 585–591.

Gamache, J. F., and R. A. Houze, 1982: Mesoscale air motions associated with a tropical squall line. *Mon. Wea. Rev.*, **110,** 118–135.

——, and ——, 1983: Water budget of a mesoscale convective system in the Tropics. *J. Atmos. Sci.*, **40,** 1835–1850.

Hoepffner, M., T. Lebel, and H. Sauvageot, 1989: EPSAT-Niger: A pilot experiment for rainfall estimation over West Africa. *Proc. WMO/IAH/ETH Int. Workshop on Precipitation Measurement,* St. Moritz, Switzerland, WMO, 251–258.

Houze, R. A., 1977: Structure and dynamics of a tropical squall-line system. *Mon. Wea. Rev.*, **105,** 1540–1567.

——, 1982: Cloud clusters and large-scale vertical motions in the Tropics. *J. Meteor. Soc. Japan,* **60,** 396–410.

——, 1989: Observed structure of mesoscale convective systems and implications for large-scale heating. *Quart. J. Roy. Meteor. Soc.*, **115,** 425–461.

——, 1993: *Cloud Dynamics.* Academic Press, 573 pp.

——, and E. N. Rappaport, 1984: Air motions and precipitation structure of an early summer squall line over the eastern tropical Atlantic. *J. Atmos. Sci.*, **41,** 553–574.

Hudlow, M. D., 1979: Mean rainfall patterns for the three phases of GATE. *J. Appl. Meteor.*, **18,** 1656–1669.

Johnson, D. B., and K. V. Beard, 1984: Oscillation energies of colliding raindrops. *J. Atmos. Sci.*, **41,** 1235–1241.

Johnson, R. H., and P. J. Hamilton, 1988: The relationship of surface features to the precipitation and air flow structure of an intense midlatitude squall line. *Mon. Wea. Rev.*, **116,** 1444–1472.

Jones, D. M. A., 1956: Rainfall drop-size distribution and radar reflectivity. Rep. No. 6, Illinois State Water Survey, Urbana, IL, 20 pp.

Joss, J., and A. Waldvogel, 1967: Ein Spektrograph für Niederschlagstropfen mit automatischer Auswertung. *Pure Appl. Geophys.*, **68,** 240–246.

——, and ——, 1969: Raindrop size distribution and sampling size errors. *J. Atmos. Sci.*, **26,** 566–569.

Kozu, T., and K. Nakamura, 1991: Rainfall parameter estimation from dual-radar measurements combining reflectivity profile and path-integrated attenuation. *J. Atmos. Oceanic Technol.*, **8,** 259–271.

Kummerow, C., I. M. Hakkarinen, H. F. Pierce, and J. A. Weinman, 1991: Determination of precipitation profiles from airborne passive microwave radiometric measurements. *J. Atmos. Oceanic Technol.*, **8,** 148–158.

Leary, C. A., 1984: Precipitation structure of the cloud clusters in a tropical easterly wave. *Mon. Wea. Rev.*, **112,** 313–325.

Mapes, B., and R. A. Houze, 1993: An integrated view of the 1987 Australian monsoon and its mesoscale convective system. Part II: Vertical structure. *Quart. J. Roy. Meteor. Soc.*, **119,** 733–754.

Marshall, J. S., and W. M. Palmer, 1948: The distribution of raindrops with size. *J. Meteor.*, **5,** 165–166.

McFarquhar, G. M., and R. List, 1993: The effect of curve fits for the disdrometer calibration on raindrop spectra, rainfall rate, and radar reflectivity. *J. Appl. Meteor.*, **32,** 774–782.

Pruppacher, H. R., and R. Rasmussen, 1979: A wind tunnel investigation of the rate of evaporation of large water drops falling at terminal velocity in air. *J. Atmos. Sci.*, **36,** 1255–1260.

Sauvageot, H., 1994: Rainfall measurement by radar: A review. *Atmos. Res.*, **35,** 27–54.

Sekhon, R. S., and R. C. Srivastava, 1971: Doppler radar observations of drop-size distributions in a thunderstorm. *J. Atmos. Sci.*, **28,** 983–994.

Sheppard, B. E., 1990: Effect of irregularities in the disdrometer classification of raindrops by the Joss–Waldvogel disdrometer. *J. Atmos. Oceanic Technol.*, **7,** 180–183.

——, and P. I. Joe, 1994: Comparison of raindrop size distribution measurements by a Joss–Waldvogel disdrometer, a PMS 2DG spectrometer, and a POSS Doppler radar. *J. Atmos. Oceanic Technol.*, **11,** 874–887.

Short, D. A., T. Kozu, and K. Nakamura, 1990: Rainrate and raindrop size distribution observations in Darwin, Australia. *Proc. URSI Commission F Open Symp. on Regional Factors in Predicting Radiowave Attenuation Due to Rain,* Rio de Janeiro, Brazil, International Union of Radio Science Commission, 35–40.

Simpson, J., R. F. Adler, and G. R. North, 1988: A proposed Tropical Rainfall Measuring Mission (TRMM) satellite. *Bull. Amer. Meteor. Soc.*, **69,** 278–295.

Sui, C. H., K. M. Lau, W. K. Tao, and J. Simpson, 1994: The tropical water and energy cycles in a cumulus ensemble model. Part I: Equilibrium climate. *J. Atmos. Sci.*, **51,** 711–728.

Tao, W. K., J. Simpson, S. Lang, M. McCumber, R. Adler, and R. Penc, 1990: An algorithm to estimate the heating budget from vertical hydrometer profiles. *J. Appl. Meteor.*, **29,** 1232–1244.

——, ——, C. H. Sui, S. Lang, J. Scala, B. Ferrier, M. D. Chou, and K. Pickering, 1993: Heating, moisture, and water budgets of tropical and mid-latitude squall lines: Comparison and sensitivity to longwave radiation. *J. Atmos. Sci.*, **50,** 673–690.

Thiele, O. W., D. A. Short, J. C. Gerlach, D. B. Wolff, M. J. McPhaden, and J. C. Wilkerson, 1994: TOGA COARE ocean precipitation morphology. Preprints, *Sixth Conf. on Climate Variations,* Nashville, TN, Amer. Meteor. Soc., J72–J75.

Tokay, A., D. A. Short, P. A. Kucera, and O. W. Thiele, 1995: On the consistency of radar Z–R relations with parameterizations of the raindrop size distribution. Preprints, *Conf. on Hydrology,* Dallas, TX, Amer. Meteor. Soc., 62–67.

Ulbrich, C. A., 1985: The effects of drop size distribution truncation on rainfall integral parameters and empirical relations. *J. Climate Appl. Meteor.*, **24,** 580–590.

Waldvogel, A., 1974: The N_0 jump of raindrop spectra. *J. Atmos. Sci.*, **31,** 1068–1078.

——, W. Henrich, and L. Mosimann, 1993: New insight into the coupling between snow spectra and raindrop size distributions. Preprints, *26th Int. Conf. on Radar Meteorology,* Norman, OK, Amer. Meteor. Soc., 602–604.

Williams, C. R., W. L. Ecklund, and K. S. Gage, 1995: Classification of precipitating clouds in the Tropics using 915-MHz wind profiler. *J. Atmos. Oceanic Technol.*, **12,** 996–1012.

Willis, P. T., 1984: Functional fits to some observed drop size distributions and parameterization of rain. *J. Atmos. Sci.*, **41,** 1648–1661.

Yuter, S. E., and R. A. Houze, 1995: Three-dimensional kinematic and microphysical evolution of Florida cumulonimbus. Part II: Frequency distributions of vertical velocity, reflectivity, and differential reflectivity. *Mon. Wea. Rev.*, **123,** 1941–1963.

Zawadski, I., and M. de Agostinho Antonio, 1988: Equilibrium raindrop size distributions in tropical rain. *J. Atmos. Sci.*, **45,** 3452–3459.